BULLETIN OF THE POLISH ACADEMY OF SCIENCES
TECHNICAL SCIENCES, Vol. 70(2), 2022, Article number: e140467
DOI: 10.24425/bpasts.2022.140467

$TE_{m,1}$ coaxial modes generator for cold-testing of high power components and devices

Grzegorz JAWORSKI*, Andrzej FRANCIK, and Kacper NOWAK

Wroclaw University of Science and Technology, Wybrzeze Wyspianskiego 27, 50-370 Wroclaw, Poland

Abstract. In this paper, we describe the development and design procedure of the new kind of coaxial $TE_{m,1}$ modes generator based on ring resonator with coupling apertures. The generator enables excitation of subsequent $TE_{m,1}$ modes in a cylindrical waveguide. The proposed design method allows to obtain high purity $TE_{m,1}$ modes. The angular mode number can be chosen by replacing the plate with coupling apertures. Structure and parameters of the generator was optimized using CST-Microwave Studio. The mode generator was fabricated and checked on the test bench in an anechoic chamber. The measured field distributions confirm excitation of the desired $TE_{m,1}$ modes. A good agreement between simulations and measurements is obtained. The presented mode generator, operating in non-rotating $TE_{m,1}$ modes, is easy to fabricate, and suitable for cold-test experiments of high power components and devices.

Key words: cold testing; high power components; microwave path; mode generator.

1. INTRODUCTION

Microwave applications such as material processing, spectroscopy of high absorbing materials and fast sub-THz imaging require high power transmission lines and beam shaping components [1–6]. Many of them rely on circular waveguides [7–9]. Errors in the design and implementation of the high power components and devices can be expensive and potentially dangerous. Any errors in such devices should be detected before applying maximum output power [10]. Due to the costs and risks associated with the high power emission the only practical option is the so-called cold test method [11–15]. This method involves measurements of important parameters at safe, low power levels. The key element of the "cold test" measuring system is a suitable low-power microwave source. The mode generator should enable the excitation of appropriate higher order azimuthal mode corresponding to this in high power component under test. A number of mode generators have been presented in literature.

A widely used method uses the converters based on the periodically perturbed waveguide wall technology [16–18]. In this method the fundamental mode is converted to the high-order waveguide mode. According to our generator concept, we found interesting solutions that use generators, operating with non-rotating $TE_{m,1}$ modes for test quasi-optical mode converters in gyrotrons. In paper [14] authors propose a new technique for testing gyrotron mode converters by using a simple, non-rotating, higher-order mode generator with $TE_{6,2}$ mode. They demonstrate the feasibility of this technique for a W-band gyrotron quasi-optical mode converter. In another paper [19] authors describe a generator consisting of a mode converter, waveguide transition, and a polarization converter that allows converting a non-rotating mod to a rotating mod. The converting process in each section is displayed and the working principles are discussed.

The main disadvantages of some proposed solutions are the complex structures which are difficult to manufacture and implement in practice. Therefore in this paper, we present new and original design of easy to fabricate mode generator operating in non-rotating whispering gallery $TE_{m,1}$ modes (WGM). The presented WGM generator is suitable for cold-test of the high power components and devices. With using appropriate mode converters, it can also be used to test devices with rotating WGM modes.

2. MODE GENERATOR THEORY AND CONSTRUCTION

The structure of $TE_{m,1}$ coaxial modes generator is presented in Fig. 1.

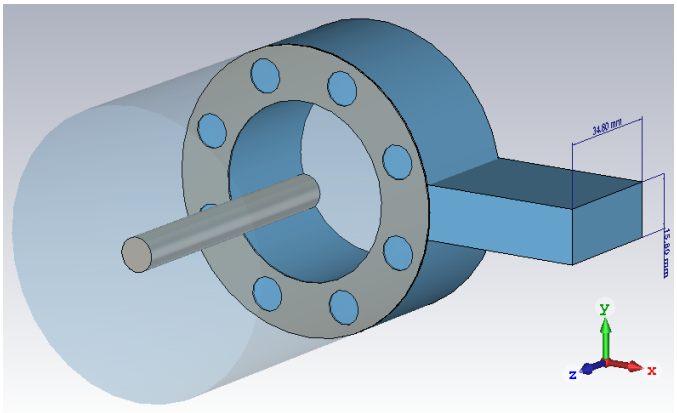

Fig. 1. Structure of the coaxial $TE_{m,1}$ modes generator

*e-mail: grzegorz.jaworski@pwr.edu.pl

Manuscript submitted 2021-08-12, revised 2021-11-20, initially accepted for publication 2021-11-29, published in April 2022.

The main component of the generator is a ring resonator with the set of coupling apertures spaced at equal intervals on the side wall of the rectangular waveguide. The ring resonator is fed through the section of waveguide connected to the ring via a waveguide E-plane T-junction. The ring resonator is connected to the circular waveguide shorted at the end through the side wall with round apertures. Round apertures allow the coupling of the standing wave in the resonator with the circular waveguide.

Additionally, a metal rod is attached in the center of the shorted end of circular waveguide to initially suppress the axial component E_z of the electric field inside waveguide (Fig. 2). The possible presence of such a component is discussed later in this paper.

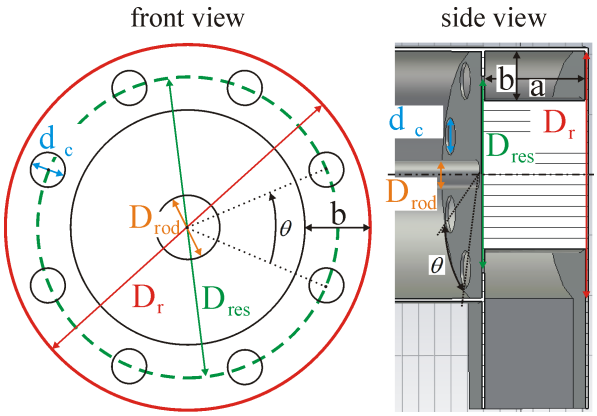

Fig. 2. D_r – cylindrical waveguide radius, D_{res} – radius defining length of the rectangular resonator/waveguide, d_c – coupling slot radius, D_{rod} – internal rod radius, θ – angle between coupling holes, b – rectangular waveguide shorter side, a – rectangular waveguide longer side

Circular waveguides support propagation of TE and TM modes. The axial and transverse components of electric and magnetic field can be written in the form presented in equations (1) to (6) where m stands for the azimuthal mode number.

$$H_z(r,\varphi,z) = H_z(0)\, J_m\left(\frac{\chi'_{m,n}}{0.5D_r}r\right)\cos(m\varphi)\, e^{-j\beta_z z}, \tag{1}$$

$$H_r(r,\varphi,z) = jH_z(0)\,\frac{\beta_z}{\beta_c}\, J'_m\left(\frac{\chi'_{m,n}}{0.5D_r}r\right)\cos(m\varphi)\, e^{-j\beta_z z}, \tag{2}$$

$$E_r(r,\varphi,z) = j\frac{m\omega\mu}{r\beta_c^2}H_z(0)\, J_m\left(\frac{\chi'_{m,n}}{0.5D_r}r\right)\sin(m\varphi)\, e^{-j\beta_z z}, \tag{3}$$

$$E_\varphi(r,\varphi,z) = j\frac{\omega\mu}{\beta_c}H_z(0)\, J'_m\left(\frac{\chi'_{m,n}}{0.5D_r}r\right)\cos(m\varphi)\, e^{-j\beta_z z}. \tag{4}$$

where

$$\beta_c = \frac{2\pi}{\lambda_c} = \frac{\chi'_{m,n}}{0.5D_r}, \tag{5}$$

$$\beta_z = \frac{2\pi}{\lambda_f}. \tag{6}$$

In Fig. 3 the examples of several subsequent axial modes $TE_{m,1}$ are presented.

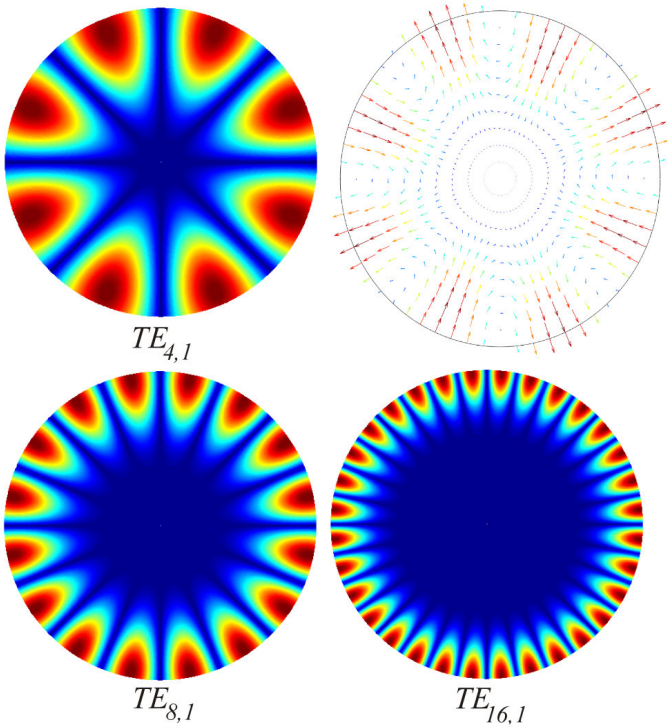

Fig. 3. Visualization of absolute values of the $TE_{m,1}$ modes calculated in MATLAB. Respectively: $TE_{4,1}$ and vector plot, $TE_{8,1}$, $TE_{16,1}$

In the developed mode generator, the well-known principle of exciting a specific field mode was applied. In appropriately selected locations, we introduce excitation by means of electric field vectors. The axial, and peripheral components of the introduced E-field vectors have directions and phases coherent to the mode we intend to excite in a circular waveguide. The number of excitation locations must be equal to the number of extremes of the field of the assumed coaxial mode in the azimuthal direction. In the case of the assumed $TE_{m,1}$ field mode, the relevant points of excitation are points evenly distributed around the circumference of the circular waveguide in places where the extrema for $TE_{m,1}$ occurs. In the excitation point for axial coordinate $z = 0$ and for $m\varphi = \frac{\pi}{2}$ components E_r and E_φ are described by equations:

$$E_r(r) \overset{(3)}{=} j\frac{m\omega\mu}{r\beta_c^2}H_z(0)\cdot J_m\left(\frac{\chi'_{m,n}}{0.5D_r}r\right), \tag{7}$$

$$E_\varphi(r) \overset{(4)}{=} 0. \tag{8}$$

It has been found that the element which enables excitation according to the described field distribution is a ring resonator made of a rectangular waveguide bent over a wider wall. A standing wave is formed in the resonator with the number of extrema equal to the number $2m$ describing the expected mode $TE_{m,1}$. In the rectangular waveguide, for the dominant mode ($TE_{1,0}$), the E-field vectors are parallel to its narrower wall with a height of b. In the case of a ring resonator E-field vectors are arranged radially in relation to the center of the resonator. The outer diameter of the ring resonator ($D_{\text{res}} + b$), where D_{res} is the mean diameter of the ring resonator, is equal to the inner

diameter of the circular waveguide D_r. Halfway up the side wall of the ring resonator (on a circle of diameter D_{res}) $2m$ round coupling apertures are positioned at distances equal to $\frac{\lambda g}{2}$ where λg is the dominant mode $TE_{1,0}$ wavelength in rectangular waveguide.

$$D_r = D_{\text{res}} + b, \tag{9}$$

where D_r – diameter of circular waveguide, b – the height of the narrower wall of the waveguide forming the ring resonator.

In order to obtain the lowest possible attenuation, the side lengths of the rectangular waveguide should meet the condition [20].

$$\frac{b}{a} = A \approx \frac{1}{2}. \tag{10}$$

Thus the center of the coupling aperture will be near the vertex of the Bessel function describing the distribution of the radial component E_r in the circular waveguide (3).

In order to obtain the most homogeneous field in the coupling aperture, its diameter d_c was assumed to be not bigger than $\frac{b}{2}$.

$$d_c \leq \frac{b}{2}. \tag{11}$$

The size of the aperture affects the coupling level and power transfer from the source to the generator. From this point of view, a larger aperture provides better coupling and better system efficiency. If we choose b lower than the optimal value described later in this paper, we can increase the hole diameter above this limit because the entire ring resonator is in the area of a approximately uniform field. Circular holes were chosen for ease of manufacture however square holes give stronger coupling with the circular waveguide and may as well be used.

The extremes of the E field radial component in the circular waveguide coincide with the extremes of the standing wave in the resonator. To meet this condition the resonator circumference must be a m multiple of the wavelength in the resonator waveguide. Hence, for $a = 2b$, the condition for the resonator diameter must be met:

$$D_{\text{res}}(\lambda_{\text{res}}) = \frac{m}{\pi}\lambda_{g_{\text{res}}} = \frac{m}{\pi}\frac{\lambda_{\text{res}}}{\sqrt{1-\left(\frac{\lambda_{\text{res}}}{4b}\right)^2}}. \tag{12}$$

3. MODE GENERATOR DESIGN

From a practical point of view the design process of the mode generator can be reduced to two basic problems.

1. Calculation of the structure parameters for **the assumed operating frequency F_{res}** and $TE_{m,1}$ mode number m.
2. Calculation of the structure parameters and operating frequency F_{res} for **a given circular waveguide diameter D_r** and $TE_{m,1}$ mode number m.

In the first case, we start from assuming mode number m and operating frequency F_{res}. On this basis, we determine the diameter D_{res} of the ring resonator and circular waveguide D_r, the rectangular waveguide size a, b and coupling apertures diameter d_c.

The operating frequency F_{res} must be within the operating frequency range Δf_{res} of the rectangular waveguide forming the ring resonator. This range is limited by the cut off frequencies for $TE_{1,0}$ dominant mode and next $TE_{2,0}$ mode.

$$\Delta f_{\text{res}} = 0.95 f_{cTE_{20}} - 1.25 f_{cTE_{10}} = 0.95\frac{c}{a} - 1.25\frac{c}{2a}. \tag{13}$$

In terms of wavelengths we can express the limits in equations (14) as:

$$\frac{\lambda_{cTE_{20}}}{0.95} < \lambda_{\text{res}} < \frac{\lambda_{cTE_{10}}}{1.25} \tag{14}$$

therefore

$$\Delta\lambda_{\text{res}} = \frac{\lambda_{cTE_{10}}}{1.25} - \frac{\lambda_{cTE_{20}}}{0.95}. \tag{15}$$

When assuming that $a = 2b$ then follows:

$$2.1\,b < \lambda_{\text{res}} < 3.2\,b, \tag{16}$$

$$\Delta\lambda_{\text{res}} \overset{(15)}{=} 1.0948\,b. \tag{17}$$

For some standard rectangular waveguides $\frac{b}{a}$ differs slightly from 2, therefore when choosing such a waveguide one should take the value of $A = \frac{b}{a}$ resulting from the waveguide size table. In that case, for standard waveguides, the formula for determining D_r has the form

$$D_r(F_{\text{res}}) = \frac{cm}{\pi F_{\text{res}}\sqrt{1-\left(\frac{cA}{F_{\text{res}}2b}\right)^2}} + b = D_{\text{res}}(F_{\text{res}}) + b. \tag{18}$$

In the second case when the diameter of the circular waveguide is fixed, for assumed mode number m we have to calculate the waveguide sizes a, b and the operating frequency F_{res}. For the given diameter of the resonator and the TE mode number m, we calculate the wavelength in the resonator and then the wavelength in free space.

$$O = 2\pi\left(\frac{D_r}{2} - \frac{b}{2}\right), \quad \lambda_g = \frac{O}{m},$$
$$\lambda_0 = \frac{\lambda_g}{\sqrt{1+\left(\frac{\lambda_g}{\lambda_{c\_wg}}\right)^2}}, \tag{19}$$

where: λ_{c_wg} – cutoff wavelength in the cylindrical waveguide for the $TE_{m,1}$ mode.

Finally, we can find operating frequency from equation:

$$F_o = \frac{c\sqrt{1+\left(\frac{\lambda_g}{\lambda_{c\_wg}}\right)^2}}{\lambda_g}. \tag{20}$$

For the assumed value of F_{res} or D_r, theoretically, there are infinitely many solutions for a given $TE_{m,1}$ mode with parameters b and A. Tests carried out with the use of the CST STUDIO electromagnetic simulator show however, that not all solutions are satisfactory. In the EM field distribution inside a circular waveguide, we can observe the presence of the axial component E_z. This means that besides TE mode also TM mode is arising. For this reason by minimizing the E_z component we are obtaining pure TE mode. This is the factor, that we use to evaluate the mode purity. The magnitude of the axial component E_z changes for different values of $\frac{b}{D_{\text{res}}}$. Various approaches of estimating the mode purity have been described in the literature [21–28]. In [28] Haas and Thumm proposed formulas for the electromagnetic field components with presence of spurious TM modes (21).

$$\begin{aligned} \vec{E} &= \vec{E}_{TE} + \psi \vec{E}_{TM}, \\ \vec{H} &= \vec{H}_{TE} + \psi \vec{H}_{TM}. \end{aligned} \tag{21}$$

In this work, the mode purity assessment was based on the analysis of the EM simulation results obtained in CST STUDIO [29]. The content of undesirable modes cannot be directly determined or identified on the basis of the CST simulation results however, we can easily obtain information about all the E-field E_x, E_y, E_z components in the waveguide. For the purposes of the evaluation of $TE_{m,1}$ mode, we assumed the value of the axial field component E_z as a proper indicator of the mode impurity. Using the CST capability, we can easily show the magnitude of the E_z and $|E|$ components on a common graph (Fig. 4). As a convenient indicator of the mode impurity, we took the ratio of components $\frac{E_z}{|E|}$ what can also be illustrated as the inclination angle of the virtual vector $|E|$ in z axis direction.

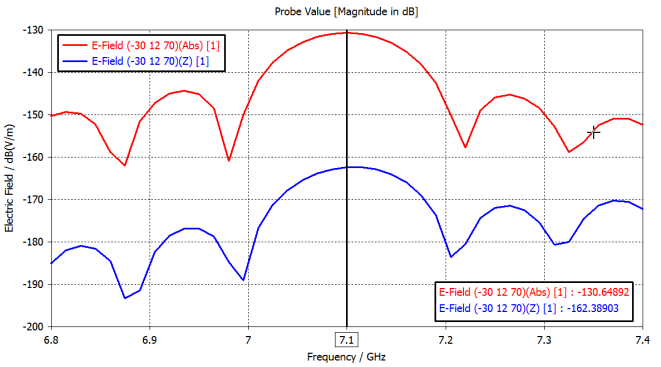

Fig. 4. CST graph of magnitude of the E-field components E_z and $|E|$

The non-zero E_z component indicates the possible presence of spurious TM modes. Figure 5a shows graphs of phase velocity as a function of operating frequency for subsequent $TE_{m,1}$ and $TM_{m,1}$ modes. In Fig. 5b the phase velocities for modes $TE_{4,1}$ and $TM_{2,1}$ are presented. The green curve shows the ΔV_p value vs. frequency.

It can be seen that both modes propagate at a very similar velocity. This is a favorable circumstance for exciting unwanted

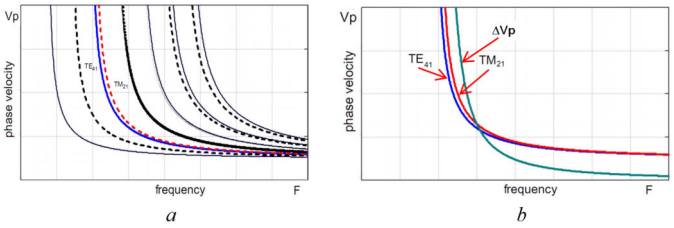

Fig. 5. Phase velocity for TE and TM modes in circular waveguide as a function of operating frequency

TM modes with E_z axial components. It can also be noticed that the difference of phase velocity ΔV or wavelength, $\Delta\lambda$ for the $TE_{m,1}$ and $TM_{m-2,1}$ varies with the the frequency. Simulations in the CST program showed that there is a clear correlation between the values of ΔV, $\Delta\lambda$ and the magnitude of the E_z component. Hence we adopted the rule that for the assumed operating frequency F_{res} , the ring resonator sidewall height b should be adjusted in such a way as to obtain a maximum values of ΔV. The difference between phase velocity ΔV for the modes $TE_{m,1}$ and $TM_{m-2,1}$ can be derived from the equation:

$$\begin{aligned} \Delta V_p(f) &= V_{pTE_{m,1}} - V_{pTM_{m-2,1}} \\ &= \frac{c}{\sqrt{1 - \frac{F_{cut_{TE_{m,1}}}}{f}}} - \frac{c}{\sqrt{1 - \frac{F_{\text{cut}_{TM_{m-2,1}}}}{f}}}. \end{aligned} \tag{22}$$

Subsequent analyses have shown that the lowest value of the E_z component is obtained when the operating frequency F_{res} is equal to the upper limit of the frequency range which is the 0.95 of cut-off frequency for the mode $TE_{2,0}$ in rectangular waveguide of the ring resonator. For this we can also calculate the minimum wavelength.

$$F_{\text{res}} = 0.95 \cdot F_{cTE_{2,0}} = 0.95 \left[\frac{c}{2\pi\sqrt{\varepsilon_r}} \sqrt{\left(\frac{2A\pi}{b}\right)^2} \right]. \tag{23}$$

For the assumed operating frequency F_{res} each time we change the value of ring resonator height b, the value of D_{res} and the relation $\frac{b}{D_{\text{res}}}$ also change. Figure 6 presents a graph showing the dependence of waveguide diameter $D_{\text{res}}(b)$ on ring resonator height b. Points A and B show the effective operating

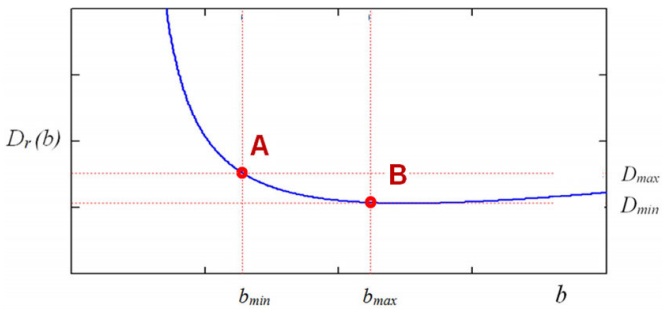

Fig. 6. Dependence of circular waveguide diameter $D_r(b)$ on ring resonator height b for given frequency F_{res}

range of the generator. Point A shows the lower limit of the b value for which the value of the E_z component exceeds the allowable limit adopted in the project. Point B shows the upper limit of the b value for which the operating frequency F_{res} is equal to the maximum frequency defined above in the operating frequency range Δf in equation 13. In terms of wavelength we can write $b_{\max}$ as:

$$b_{\max} = 0.95A\lambda_{\text{res}}\,. \tag{24}$$

4. SUMMARY OF THE *TE* MODES GENERATOR DESIGN WITH DIAGRAMMATIC METHOD

The summary of generator design process can be illustrated in the standardized graphs shown in Fig. 7. It shows the graphs of the functions y_1, y_2, y_3, y_4, y_5, y_6 for mode number $m = 4$. In order to facilitate the graphical presentation on the diagram, normalization of curves to b and wavelength λ_{res} has been introduced. The condition for the circular waveguide diameter $D_r\,(\lambda_{\text{res}})$ can be written in normalized form as:

$$y_4 = \frac{D_r(\lambda_{\text{res}})}{b} = \frac{4m}{\pi}\cdot\frac{1}{\sqrt{\left(\frac{4}{x}\right)^2 - 1}} + 1, \tag{25}$$

where: $x = \dfrac{\lambda_{\text{res}}}{b}$.

In terms of wavelengths we can express the limits of operation as:

$$\frac{\lambda_{cTE_{20}}}{0.95} < \lambda_{\text{res}} < \frac{\lambda_{cTE_{10}}}{1.25} \tag{26}$$

or, for $a = 2b$,

$$2.1b < \lambda_{\text{res}} < 3.2b \tag{27}$$

and

$$\Delta\lambda_{\text{res}} \overset{(26,27)}{=} \frac{\lambda_{cTE_{10}}}{1.25} - \frac{\lambda_{cTE_{20}}}{0.95} = 3.2b - 2.1053b = 1.0948b. \tag{28}$$

In normalized form the relationship between wavelength and ring resonator height b can be written:

$$2.1 < \frac{\lambda_{\text{res}}}{b} < 3.2, \frac{\Delta\lambda_{\text{res}}}{b} = 1.0948. \tag{29}$$

To ensure the conditions for excitation only the dominant mode ($TE_{1,0}$) in the resonator the $x = \dfrac{\lambda_{\text{res}}}{b}$ must be set in the range of (2.1, 3.2): $x_A \in (2.1, 3.2)$. Then the ratio $y_4 = \dfrac{D_r}{b}$ should be determined from the formula:

$$y_{4_A} = \frac{4m}{\pi}\cdot\frac{1}{\sqrt{\left(\frac{4}{x_A}\right)^2 - 1}} + 1. \tag{30}$$

Next the values of b_A and a_A can be calculated:

$$b_A = \frac{D_{r_A}}{y_{4_A}}, \quad a_A = 2b_A \tag{31}$$

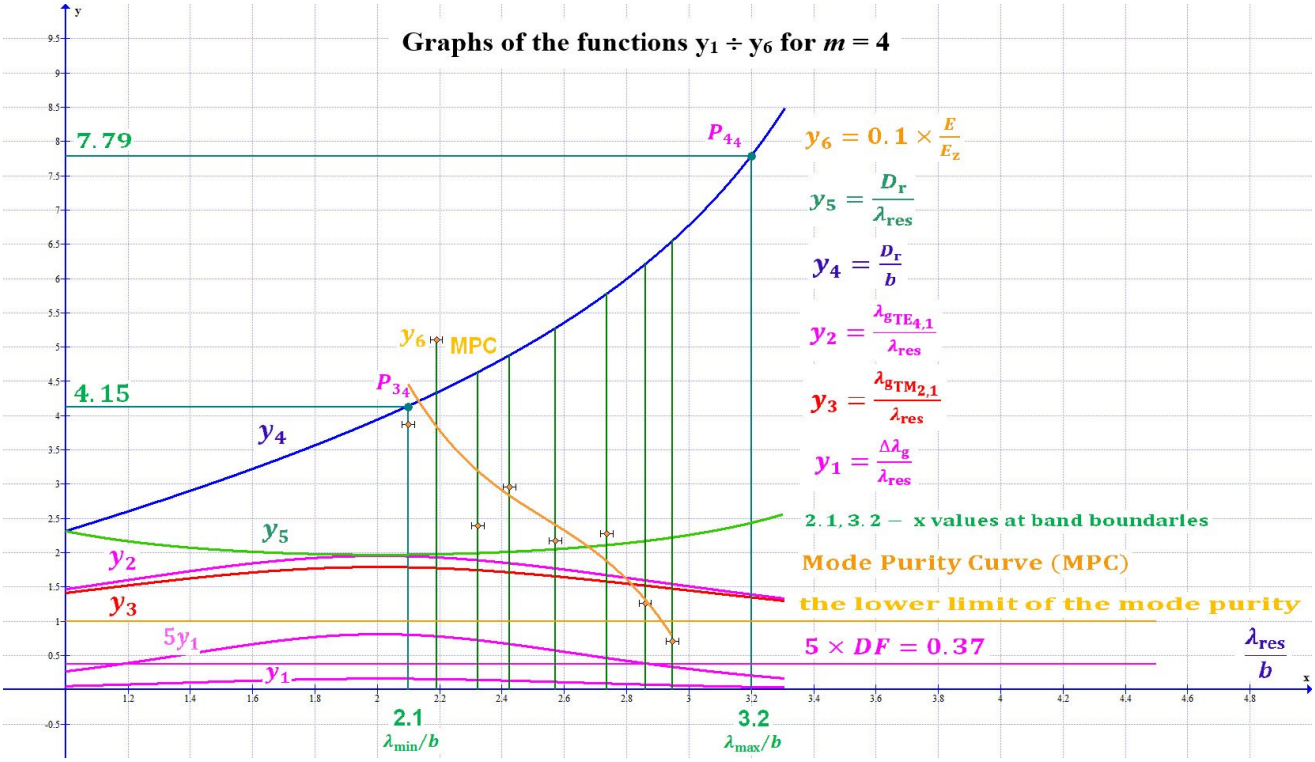

Fig. 7. Generator design with diagrammatic method

and

$$\lambda_{\text{res}A} = x_A \cdot b_A\,, \tag{32}$$

$$F_{\text{res}A} = \frac{c}{\lambda_{res_A}}\,. \tag{33}$$

For better visualization, the normalization of these charts has been introduced. The ordinate axis x is normalized to $\frac{\lambda_{\text{res}}}{b}$. The points P_{34} and P_{44} represent values of $\left(\frac{D_r}{b}\right)$ at the boundaries of the resonator waveguide operating band. **The design process of the generator can be reduced to the search for the maximum value of $\Delta\lambda_{g_{\text{res}}}$ in the operating band of the ring resonator waveguide.**

This is illustrated by curves y_1, $5y_1$ and y_2, y_3. The y_2 (pink) and y_3 (red) curves shows the wavelength for $TE_{4,1}$ and $TM_{2,1}$ modes referred to λ_{res} while y_1 curve shows the difference between these normalized wavelengths. The y_4 (blue) curve shows the basic relationship used in the generator design process, linking the diameter of a circular waveguide D_r, matched to the diameter D_{res} of the resonator, with the resonant wavelength of the resonator λ_{res}. The mode purity curve (MPC) is a trend line showing the improvement of the mode purity index $y_6 = \frac{E}{E_z}$, where E – modulus of the field resultant vector E, with decreasing values of λ_{res}/b. The MPC line was determined on the basis of the CST simulation for different values of $\frac{D_r}{b}$. $y_5 = \frac{D_r}{\lambda_{\text{res}}}$ is a curve informing about the possibility of using the RT method to analyze the generator operation, when high order axial modes and high frequencies are applied. The obvious criterion allowing the use of the RT method to analyze wave propagation in the generator circular waveguide is the requirement that $y_5 > 10$, which means that the diameter of the waveguide is 10 times the wavelength.

5. SIMULATION RESULTS

In order to verify the proposed design method a virtual model of the generator was implemented in CST Microwave Studio [29]. Figure 8 shows the results of the E-field simulation in the plane perpendicular to the Z axis.

The field distribution characteristic of the $TE_{4,1}$ mode is clearly visible. In Fig. 9 excitation and propagation of the mode

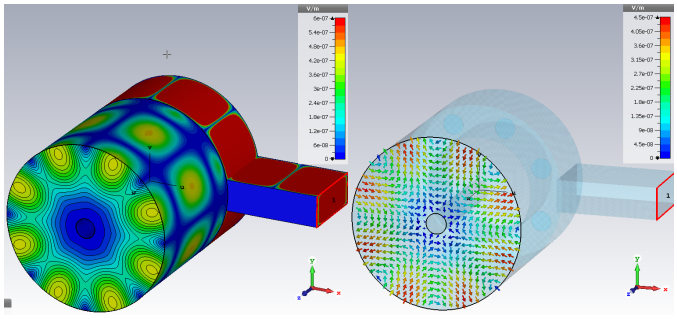

Fig. 8. E-field distribution in a cross-section perpendicular to the Z axis

$TE_{4,1}$ along Z axis can be observed. All E-field vectors are perpendicular to the Z axis which is what can be expected for the transverse TE modes.

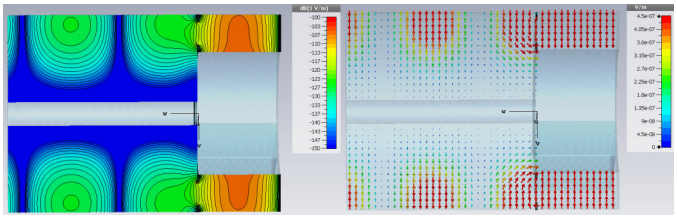

Fig. 9. E-field for propagation of the mode $TE_{4,1}$ along the circular waveguide the z axis

In Fig. 10 the E-field distribution for the higher order modes $TE_{8,1}$ and $TE_{16,1}$ are presented.

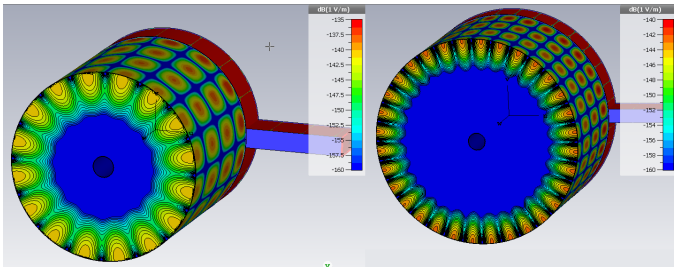

Fig. 10. Simulation of the E-field distribution for the modes $TE_{8,1}$ and $TE_{16,1}$

The simulations were performed to show the possibility of exciting propagation of higher order mods for high frequency applications. When the diameter of the waveguide is 10 times the wavelength the RT method can be applied to analyze wave propagation and design mode converters [30, 31]. The possibility of exciting such modes is limited by the manufacturing and assembling precision of the generator elements.

6. EXPERIMENTAL VERIFICATION OF THE MODEL

In a practical implementation, the resonator structure has been milled into a metal block which is shown in Fig. 11. In order to facilitate the manufacturing and measurement process, the standard size of the circular waveguide C25 and mode number $TE_{4,1}$ were adopted. The generator model was built in accordance with the assumptions and theory described in part III.

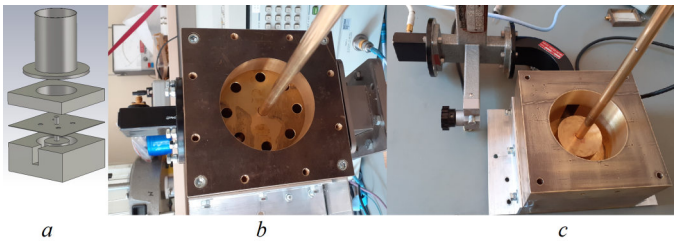

a *b* *c*

Fig. 11. The practical implementation of the resonator structure

In Fig. 11 the model of the generator structure with the main components like ring resonator, rectangular waveguide and circular waveguide is presented. Such a solution allows the use of the same resonator ring and circular waveguide to excite different $TE_{m,1}$ modes on different frequencies only by replacing the plate with coupling apertures (shown in Fig. 11 a, b).

An impedance matching circuit with a waveguide tuner is placed at the input of the ring resonator to provide maximum power transfer from signal generator to the mode generator. Since the measurement of the E-field inside the circular waveguide may cause disturbances in the field distribution, it was decided to perform measurements at the circular waveguide output aperture. In order to avoid mismatch at the end of the waveguide, a tube cone was used which allows a gentle transition to the impedance of free space and smooth radiation of the EM wave generated in the waveguide. Figure 12 shows the generator model on the test bench (a) and in the anechoic chamber (b). Figure 12c shows the planar scanner setup with the probe placed on the extension arm.

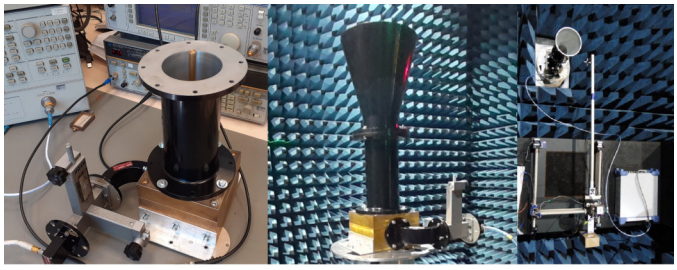

a *b* *c*

Fig. 12. Manufactured generator model on the test bench, in the anechoic chamber with the tube cone attached (far field measurement) and planar scanner setup (near field measurement) respectively

The field measurements in the cone aperture were made using two methods: Near field measurements using a planar scanner and measurements in upper hemisphere using spherical scanner. In this method, the distribution of the magnetic current density on the surface of the virtual sphere surrounding the measured object is determined. In the next step, the density of surface currents is converted into the E field distribution in the nearfield region [32]. Figure 13 shows the CST simulation results compared to the measurement result obtained on the planar scanner. Both the simulations and the measurements show the field distribution at 2 cm above the output aperture of tube cone. The asymmetry in the field distribution results from imperfect measurements setup. The asymmetry remains in the same place also after rotating the measured mode generator by 90 or 180 degree which means that the asymmetry is not related to the structure of the generator.

Figure 14 shows the far field radiation characteristics measured with the spherical scanner and the results of its transformation to the near field region. We can observe eight lobes corresponding to the field maxima near the aperture surface. All these results confirm the excitation of the $TE_{4,1}$ mode in the

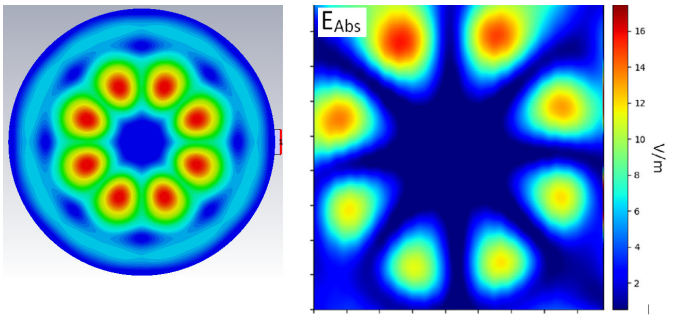

a *b*

Fig. 13. On the CST simulation of the E-field distribution at 2 cm above the output aperture on the left hand side and planar scanner results on the right hand side

circular waveguide. The agreement of measurements with the simulation results presented is fairly good.

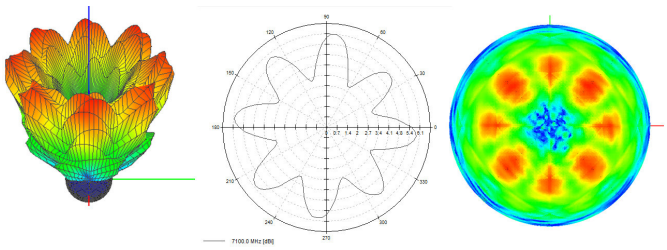

Fig. 14. The far field radiation characteristics measured with spherical scanner and the results of transformation to the near field region (right hand side)

7. CONCLUSION

The $TE_{m,1}$ modes can be easily launched in circular waveguide with a new type of the coaxial mode generator, which uses a ring resonator with coupling apertures to excite the propagation of the desired $TE_{m,1}$ mode. A number of subsequent $TE_{m,1}$ modes can be excited in the same setup just by replacing the single metal plate with coupling apertures. The proposed design method allows for launching a high purity modes. We proposed a method of designing generator structural parameters for the assumed operating frequency as well as determining the operating frequency for selected structural parameters of the generator. The presented mode generator is easy to fabricate, and suitable for cold-test experiments of high power components and devices operating in non-rotating and rotating whispering gallery $TE_{m,1}$ modes.

REFERENCES

[1] D. Wagner, M. Thumm, G. Gantenbein, W. Kasparek, and T. Idehara, "Analysis of a Complete Gyrotron Oscillator Using the Scattering Matrix Description," *Int. J. Infrared Millimeter Waves*, vol. 19, pp. 185–194, 1998, doi: 10.1023/A:1022515506809.

[2] T. Trzcinski, N. Palka, and M. Szustakowski, "THz spectroscopy of explosive-related simulants and oxidizers," *Bull. Pol. Acad. Sci. Tech. Sci.*, vol. 59, no. 4, pp. 445–447, Dec. 2011, doi: 10.2478/v10175-011-0056-4.

[3] D. Nowak, B. Gal, A. Wlodarska, and K. Granat, "The Influence of Microwave Drying Parameters on the Properties of Synthetic Moulding Sands," *Arch. Foundry Eng.*, vol. 19, no. 4, pp. 51–54, 2019, doi: 10.24425/afe.2019.129629.

[4] D. Nowak, "The Impact of Microwave Penetration Depth on the Process of Heating the Moulding Sand with Sodium Silicate," *Arch. Foundry Eng.*, vol. 17, no. 4, pp. 115–118, Dec. 2017, doi: 10.1515/afe-2017-0140.

[5] K. Rajewska, A. Smoczkiewicz-Wojciechowska, and J. Majka, "Intensification of beech wood drying process using microwaves," *Chem. Process Eng.*, vol. 40, no. 2, pp. 179–187, 2019, doi: 10.24425/CPE.2019.126110.

[6] J. Cieslik, V. Kismereshkin, E. Ritter, A. Savostin, D. Ritter, and N. Nabiyev, "Installation for Concentrated Uniform Heating of Objects by Microwave Radiation," *Int. J. Electron. Telecomm.*, vol. 66, no. 2, pp. 295–300, 2020, doi: 10.24425/IJET.2020.131877.

[7] N.L. Aleksandrov *et al.*, "Selective excitation of high-order modes in circular waveguides," *Int. J. Infrared Millimeter Waves*, vol. 13, no. 9, pp. 1369–1385, Sep. 1992, doi: 10.1007/BF01009994.

[8] M. Hruszowiec *et al.*, "The Microwave Sources for EPR Spectroscopy," *J. Telecomm. Inf. Technol.*, no. 2, pp. 18–25, Jul. 2017, doi: 10.26636/jtit.2017.107616.

[9] E. Plinski, "Gorky's Gyrotron Heroes," *Bull. Pol. Acad. Sci. Tech. Sci.*, vol. 68, no. 6, pp. 1257–1262, 2020, doi: 10.24425/bpasts.2020.135392.

[10] T. Rzesnicki *et al.*, "2.2-MW Record Power of the 170-GHz European Preprototype Coaxial-Cavity Gyrotron for ITER," *IEEE Trans. Plasma Sci.*, vol. 38, no. 6, pp. 1141–1149, Jun. 2010, doi: 10.1109/TPS.2010.2040842.

[11] P.J. Castro, J.J. Barroso, R.A. Correa, and M.C.A. Nono, "Cold tests of A 10-GHz gyrotron cavity," *Int. J. Infrared Millimeter Waves*, vol. 13, no. 1, pp. 91–104, Jan. 1992, doi: 10.1007/BF01011210.

[12] A. Arnold, G. Dammertz, and M. Thumm, "Low power tests on a TE/sub 28.8/-gyrotron mode converter system," in *25th International Conference on Infrared and Millimeter Waves*, Beijing, China, 2000, pp. 185–186, doi: 10.1109/ICIMW.2000.892992.

[13] V. Yadav *et al.*, "Cold test of cylindrical open resonator for 42 GHz, 200 kW gyrotron," *Sadhana*, vol. 38, no. 6, pp. 1347–1356, Dec. 2013, doi: 10.1007/s12046-013-0156-y.

[14] S.G. Kim, D.S. Kim, M.S. Choe, W. Lee, J. So, and E.M. Choi, "Cold testing of quasi-optical mode converters using a generator for non-rotating high-order gyrotron modes," *Rev. Sci. Instrum.*, vol. 85, no. 10, p. 104709, Oct. 2014, doi: 10.1063/1.4898180.

[15] G. Jaworski, A. Francik, M. Nowak, and K. Nowak, "Review of Experimental Verification Methods of Gyrotron Quasi-optical Mode Converters," *J. Telecomm. Inf. Technol.*, vol. 3, pp. 75–85, Oct. 2020, doi: 10.26636/jtit.2020.141320.

[16] M. Thumm, "High-power millimetre-wave mode converters in overmoded circular waveguides using periodic wall perturbations," *Int. J. Electron.*, vol. 57, no. 6, pp. 1225–1246, Dec. 1984, doi: 10.1080/00207218408938998.

[17] M. Buckley and R. Vernon, "Compact quasi-periodic and aperiodic TE/sub 0n/ mode converters in overmoded circular waveguides for use with gyrotrons," *IEEE Trans. Microwave Theory Tech.*, vol. 38, no. 6, pp. 712–721, Jun. 1990, doi: 10.1109/22.130965.

[18] W. Lawson, M. Arjona, B. Hogan, and R. Ives, "The design of serpentine-mode converters for high-power microwave applications," *IEEE Trans. Microwave Theory Tech.*, vol. 48, no. 5, pp. 809–814, May 2000, doi: 10.1109/22.841875.

[19] Z. Wu, H. Li, B. Hu, J. Xu, and T. Li, "Design of a circular $TE_{5,1}$ mode generator for gyrotrons low-power measurement," *J. Electromagn. Waves Appl.*, vol. 27, no. 13, pp. 1660–1671, Sep. 2013, doi: 10.1080/09205071.2013.822338.

[20] K.H. Yeap, C.Y. Tham, G. Yassin, and K.C. Yeong, "Attenuation in Rectangular Waveguides with Finite Conductivity Walls," *Radioengineering*, vol. 20, no. 2, p. 7, 2011.

[21] M. Pereyaslavets, O. Braz, S. Kern, M. Losert, A. Mobius, and M. Thumm, "Improvements of mode converters for low-power excitation of gyrotron-type modes," *Int. J. Electron.*, vol. 82, no. 1, p. 11, 1997, doi: 10.1080/002072197136291.

[22] A. Kapoor and G. Singh, "Mode classification in cylindrical dielectric waveguides," *J. Lightwave Technol.*, vol. 18, no. 6, pp. 849–852, Jun. 2000, doi: 10.1109/50.848397.

[23] S. Jawla, J.-P. Hogge, S. Alberti, T. Goodman, B. Piosczyk, and T. Rzesnicki, "Infrared Measurements of the RF Output of 170-GHz/2-MW Coaxial Cavity Gyrotron and Its Phase Retrieval Analysis," *IEEE Trans. Plasma Sci.*, vol. 37, no. 3, pp. 414–424, Mar. 2009, doi: 10.1109/TPS.2008.2011488.

[24] M. Losert, J. Jin, and T. Rzesnicki, "RF Beam Parameter Measurements of Quasi-Optical Mode Converters in the mW Range," *IEEE Trans. Plasma Sci.*, vol. 41, no. 3, pp. 628–632, Mar. 2013, doi: 10.1109/TPS.2012.2232942.

[25] P.C. Kalaria *et al.*, "Mode purity estimation of the gyrotron RF beam," in *2013 38th International Conference on Infrared, Millimeter, and Terahertz Waves (IRMMW-THz)*. Mainz, Germany: IEEE, Sep. 2013, pp. 1–2, doi: 10.1109/IRMMW-THz.2013.6665414.

[26] T. Ruess *et al.*, "Computer-Controlled Test System for the Excitation of Very High-Order Modes in Highly Oversized Waveguides," *J. Infrared Millimeter Terahertz Waves*, vol. 40, no. 3, pp. 257–268, Mar. 2019, doi: 10.1007/s10762-018-0566-3.

[27] D. Haas, M. Thumm, and J. Jelonnek, "Calculations on Mode Eigenvalues in a Corrugated Waveguide with Varying Diameter and Corrugation Depth," *J. Infrared Millimeter Terahertz Waves*, Apr. 2021, doi: 10.1007/s10762-021-00791-w.

[28] D. Haas and M. Thumm, "Design Procedure for a Broadband TE11/HE11 Mode Converter for High-Power Radar Applications," *J. Infrared Millimeter Terahertz Waves*, vol. 42, no. 4, pp. 380–390, Apr. 2021, doi: 10.1007/s10762-021-00773-y.

[29] S. Dassault. Cst microwave studio. [Online]. Available: https://www.3ds.com/products-services/simulia/products/cst-studio-suite/

[30] J. Jin, "Quasi-Optical Mode Converter for a Coaxial Cavity Gyrotron," Ph.D. dissertation, Institut fur Hochleistungsimpuls und Mikrowellentechnik, Forschungszentrum Karlsruhe GmbH, 2007.

[31] A. Francik, G. Jaworski, M. Nowak, and K. Nowak, "Vlasov Launcher Diagrammatic Design Using the RT Method," *J. Telecomm. Inf. Technol.*, vol. 2, pp. 57–67, Mar. 2021, doi: 10.26636/jtit.2021.150321.

[32] P.F. Wacker, "Near-field antenna measurements using a spherical scan: Efficient data reduction with probe correction," in *Inst. Elec. Eng. Conf. Publ. 113 Conf. Precision Electromagn. Measurements*, vol. 113, London, Jul. 1974, pp. 286–288.